Journal of Power Sources 185 (2008) 345–355

Contents lists available at ScienceDirect

Journal of Power Sources

journal homepage: www.elsevier.com/locate/jpowsour

Development of a novel computational tool for optimizing the operation of fuel cells systems: Application for phosphoric acid fuel cells

P.L. Zervas, A. Tatsis, H. Sarimveis*, N.C.G. Markatos

National Technical University of Athens, School of Chemical Engineering, 9 Heroon Polytechniou Street, GR-157 80 Athens, Greece

ARTICLE INFO

Article history:
Received 29 February 2008
Received in revised form 19 May 2008
Accepted 22 June 2008
Available online 9 July 2008

Keywords:
Fuel cells
CFD
Modeling
Optimization
Neural networks

ABSTRACT

Fuel cells offer a significant and promising clean technology for portable, automotive and stationary applications and, thus, optimization of their performance is of particular interest. In this study, a novel optimization tool is developed that realistically describes and optimizes the performance of fuel cell systems. First, a 3D steady-state detailed model is produced based on computational fluid dynamics (CFD) techniques. Simulated results obtained from the CFD model are used in a second step, to generate a database that contains the fuel and oxidant volumetric rates and utilizations and the corresponding cell voltages. In the third step mathematical relationships are developed between the input and output variables, using the database that has been generated in the previous step. In particular, the linear regression methodology and the radial basis function (RBF) neural network architecture are utilized for producing the input–output "meta-models". Several statistical tests are used to validate the proposed models. Finally, a multi-objective hierarchical Non-Linear Programming (NLP) problem is formulated that takes into account the constraints and limitations of the system. The multi-objective hierarchical approach is built upon two steps: first, the fuel volumetric rate is minimized, recognizing the fact that our first concern is to reduce consumption of the expensive fuel. In the second step, optimization is performed with respect to the oxidant volumetric rate. The proposed method is illustrated through its application for phosphoric acid fuel cell (PAFC) systems.

1. Introduction

A fuel cell is a device where chemical energy from a fuel, such as hydrogen, is electrochemically converted to electrical and thermal energy, without the need for combustion and without producing noise or pollution. Performance optimization is a primary target of the fuel cell technology that can substantially increase its competitiveness and benefits in industrial, automotive and environmental applications.

Fuel cells offer a significant and promising clean technology, but they are governed by complex multi-physics phenomena, that can be modeled only by advanced modeling tools. Among several alternative techniques, computational fluid dynamics (CFD) models have been used extensively for simulating the static and/or dynamic operation of fuel cells [1–4]. However, most modeling techniques suffer from long simulation running times. Mathematical meta-models based on CFD results [5] can noticeably increase simulation speed. Neural network models (NNM) have been used with success to develop such meta-modeling relationships between input and output variables [6]. Recent research has shown that neural network approaches can produce simulation results of high accuracy and reliability, whereas at the same time the computational times are reduced significantly [7,8]. Moreover, NNM applications are considered as a practical and alternative methodology to analytical and empirical models of fuel cells [9].

In this paper, we present a novel method for examining and optimizing the performance of fuel cell systems based on a meta-modeling approach. Initially, a detailed 3D steady-state, isothermal CFD simulation model [10] of the fuel cell system is used to generate a database that contains the values of the key system variables: the fuel and oxidant volumetric rates and utilizations and the

Abbreviations: 3D, three-dimensional; CFD, computational fluid dynamics; CPU, central processor unit; FC, fuel cell; LHV, lower heating value; LOO, leave one out; NLP, Non-Linear Programming; NNM, neural network model; OCV, open circuit voltage; PAFC, phosphoric acid fuel cell; PEMFC, proton exchange membrane fuel cell; PRESS, prediction error sum of squares; RAM, random access memory; RBF, radial basis function; RMSE, root mean-squared error; SOFC, solid oxide fuel cell; SSE, sum of squared errors between the observations and the predicted values; SSY, sum of squared deviations between the observations and their mean; STP, standard temperature and pressure conditions.

* Corresponding author at: National Technical University of Athens, School of Chemical Engineering, Zografou University Campus, 15780 Athens, Greece.
Tel.: +30 210 7723237; fax: +30 210 7723138.
E-mail address: hsarimv@chemeng.ntua.gr (H. Sarimveis).

0378-7753/$ – see front matter © 2008 Elsevier B.V. All rights reserved.
doi:10.1016/j.jpowsour.2008.06.081

Nomenclature

A	Tafel constant (V)
A_{eff}	electrode effective area (m^2)
C_i	concentration of component i, where i are components of a gas mixture ($kg_i\ kg_{mix}^{-1}$)
$D_{i,\text{mix}}$	mixture molar diffusivity ($m^2\ s^{-1}$)
D_{ij}	binary diffusivities for each pair of chemical species in gas mixture ($m^2\ s^{-1}$)
E	reversible open circuit voltage given by Nernst equation (V)
I	current density ($A\ m^{-2}$)
I^*	optimal value of current density ($A\ m^{-2}$)
I_0	exchange current density ($A\ m^{-2}$)
k	number of independent variables
L	number of hidden nodes in the neural network topology
m	constant in the empirical equation for mass concentration losses (V)
$m_{H_2,\text{input}}$	mass of fuel input in cell ($kg\ s^{-1}$)
$m_{H_2,\text{react}}$	mass of fuel reacted in cell ($kg\ s^{-1}$)
$m_{O_2,\text{input}}$	mass of oxidant reacted in cell ($kg\ s^{-1}$)
$m_{O_2,\text{react}}$	mass of oxidant input in cell ($kg\ s^{-1}$)
n	number of the available data
n_c	constant in the empirical equation for mass concentration losses ($m^2\ A^{-1}$)
n_{eff}	fuel cell efficiency (%)
n^*_{eff}	optimal value of fuel cell efficiency (%)
P_C	fuel cell output power (W)
P_D	power demand (W)
PD	power density ($W\ m^{-2}$)
PD*	optimal value of power density ($W\ m^{-2}$)
Q_f	inlet fuel gas volumetric rate ($l\ h^{-1}$)
Q_f^1	value of the inlet fuel gas volumetric rate after the first stage of the optimization problem ($l\ h^{-1}$)
Q_f^*	optimal value of the inlet fuel gas volumetric rate ($l\ h^{-1}$)
Q_{ox}	inlet oxidant gas volumetric rate ($l\ h^{-1}$)
Q_{ox}^*	optimal value of the inlet oxidant gas volumetric rate ($l\ h^{-1}$)
r	area specific resistance ($\Omega\ m^{-2}$)
R^2	coefficient of determination (%)
R^2_{CV}	coefficient of determination by using the cross-validation technique (%)
S_ϕ	source term of ϕ variable
$\vec{u}$	velocity vector
U_f	hydrogen utilization (%)
U_f^*	optimal value of hydrogen utilization (%)
U_{ox}	oxygen utilization (%)
U_{ox}^*	optimal value of oxygen utilization (%)
V_C	cell voltage (V)
$\bar{V}_C$	mean of all CFD cell voltage values in the available dataset
V_C^*	optimal value of cell voltage (V)
$V_{C,i}$	CFD cell voltage value for observation i (V)
$\hat{V}_{C,i}$	model prediction of cell voltage for observation i (V)
$\hat{V}^{\text{LOO}}_{C,i}$	cell voltage prediction for observation i of the model that is trained using all the available data, except for observation i
ΔV_{act}	activation losses (V)
ΔV_{conc}	concentration losses (V)
ΔV_{losses}	cell voltage losses (V)
ΔV_{ohm}	ohmic losses (V)
w_j	the weight corresponding to the response of the jth node in the neural network topology
$\mathbf{x}_j$	the centre of the jth node in the neural network topology
$\mathbf{x}$	input vector in the neural network model
X_j	Molar fraction of mixture component j
z_j	The response of the jth node in the neural network topology

Greek symbols

α	charge transfer coefficient (typical value 0.5)
β_f	coefficient in the definition of hydrogen utilization
β_{ox}	coefficient in the definition of oxygen utilization
Γ_ϕ	exchange coefficient
Γ_{C_i}	exchange coefficient representing the diffusivity for each mixture component ($kg\ m^{-1}\ s^{-1}$)
θ	tuning parameter in the formulation of the multi-objective optimization problem
μ_{mix}	viscosity of the mixture (Pa s)
ρ	density of the mixture ($kg\ m^{-3}$)
ϕ	dependent variable, i.e. U, V, W, C_i, and 1 for continuity

corresponding cell voltages. These values are obtained after several runs of the CFD model. Linear regression is then applied to develop a linear correlation model between the input and the output variables, while an advanced NNM methodology is applied to obtain a non-linear model. The database is also used for validating the accuracy of both linear and non-linear models. Eventually, a hierarchical multi-objective optimization problem is formulated, that can be used with both linear and non-linear approaches, in order to obtain the optimal values of the decision variables, i.e. the fuel and oxidant volumetric flows. The proposed computational tool is illustrated through its application for phosphoric acid fuel cell (PAFC) systems and is summarized graphically in Fig. 1.

2. PAFC simulation

2.1. CFD modeling

2.1.1. The physical problem

PAFCs belong to the medium operation temperature fuel cells (~220 °C). The type of the electrolyte that is used in a PAFC permits and facilitates the conduction of mobile H^+ ions. Air or pure oxygen is used as the oxidant gas, while pure hydrogen or a gas mixture that contains hydrogen and carbon dioxide (produced by hydrocarbon reforming) is used as fuel gas.

Reactions taking place in a PAFC are the following:

$$\textit{Anode}: \quad 2H_2 \rightarrow 4H^+ + 4e^- \tag{1}$$

$$\textit{Cathode}: \quad O_2 + 4H^+ + 4e^- \rightarrow 2H_2O \tag{2}$$

$$\text{Total reaction}: \quad H_2 + \tfrac{1}{2}O_2 \rightarrow H_2O \tag{3}$$

In the PAFC system considered in this work, the content of the anode electrode is 10 wt% Pt/C of catalyst powder, while for the cathode the catalyst powder used contains 25 wt% Pt/C. The fuel gas and the oxidant gas enter the PAFC in cross-flow. The fuel gas flows in the longer electrode and the oxidant gas in the shorter one, when an orthogonal cell is considered. The examined fuel cell geometry is given in Table 1.

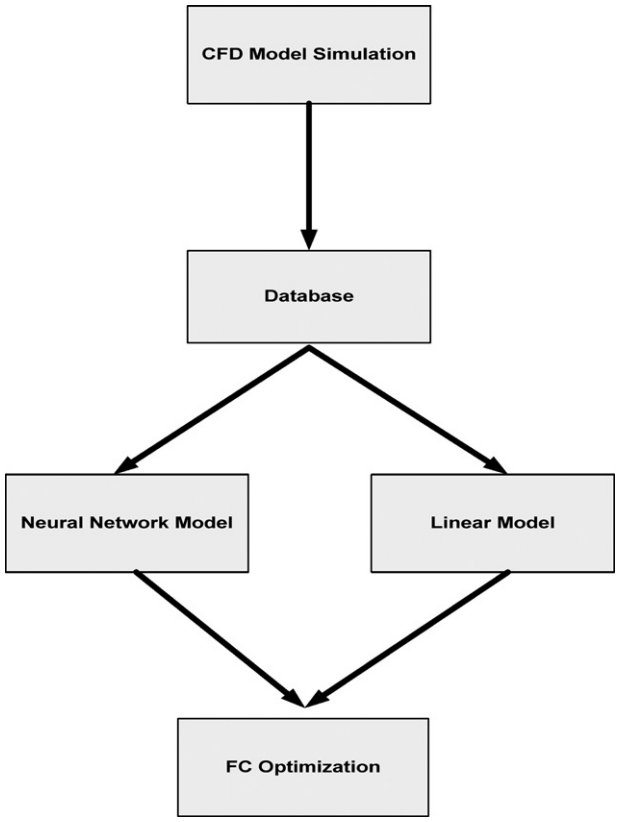

Fig. 1. Flowchart of the proposed PAFC modeling and optimization procedure.

The thickness of the electrolyte including the electrodes is 3 mm, the thickness of half bipolar plate is 0.5 mm and the thickness of gas flow channels is 3 mm. The half bipolar plate is considered for a single cell simulation. The fuel cell geometry is chosen from an experimental fuel cell performance study, in order to compare the numerical results with the experimental data [11].

A non-uniform grid was used to minimize the computational requirements while allowing proper resolution in high-gradient regions (near wall regions; electrodes). Detailed numerical tests were performed to ensure that the solutions were independent of the grid size. A $51 \times 33 \times 45$ mesh was found to provide sufficient spatial resolution and give a grid-independent solution.

The average time required for a run, with the above mesh, is about 4.5 h on a Silicon Graphics Server Origin 200, 2 CPU R 10,000, 384 MB.

2.1.2. The mathematical model

Since the purpose of this work is the development of a useful computational tool, simple physics have been introduced for demonstration purposes. It should be emphasized, however, that physics of any complexity might be easily introduced into the developed computational framework. Due to the PAFC geometry a Cartesian coordinate system is used. As it has already been mentioned above, grid independency study results have indicated a computational grid that consists of $51 \times 33 \times 45$ (NX × NY × NZ) cells. Mathematical analysis is based on the set of elliptic partial differential equations of mass and momentum conservation and chemical species composition, when a steady-state 3D flow is considered. The governing equations of every dependent variable ϕ can be expressed in the following generic form [12]:

$$\frac{\partial}{\partial t}(\rho\phi) + \mathrm{div}(\rho\vec{u}\phi) = \mathrm{div}(\Gamma_\phi \mathrm{grad}\phi) + S_\phi \quad (4)$$

where ρ is the mixture's density, $\vec{u}$ is the velocity vector, Γ_ϕ is the exchange coefficient and S_ϕ is the source term representing the production or consumption rate of each component. The SIMPLEST algorithm of the commercial CFD code PHOENICS® is used to solve the partial differential equations set [13].

The following assumptions are made in the model: (a) steady-state; (b) ideal-gas mixtures; (c) incompressible and laminar flow due to law gas velocities (Reynolds number based on the hydraulic diameter is of order 10); (d) isothermal operation (valid only for the cell and not for the stack); (e) electrochemical procedures are considered to be described adequately by Faraday's first law; (f) oxidant and fuel never get in contact as they flow in different channels and they are separated by the two solid electrodes.

Gas mixture density is calculated by the ideal-gas law and mixture viscosity is calculated by Wilke's formula [14]. The diffusion coefficients $D_{i,\mathrm{mix}}$ for multi-component flow are calculated from the following equation:

$$D_{i,\mathrm{mix}} = \left(\sum_{\substack{j=1 \\ j \neq i}}^{5} \frac{X_j}{D_{ij}} \right)^{-1} \quad (5)$$

where X_j represents the mole fractions of the different components in the gas mixture, and D_{ij} are the binary diffusivities for each pair of chemical species in the mixture. It should be mentioned here that since the flow is laminar, Γ_{C_i} is equal to $\rho D_{i,\mathrm{mix}}$ [15].

2.1.3. Boundary and special internal conditions

Boundary conditions must be specified at the inlets, outlets and walls, and special internal conditions must be set at the surfaces of the electrodes. Inlet mass fractions for the chemical species are ($\mathrm{kg}_i/\mathrm{kg}_{mix}$):

- *Anode*: H_2 0.25, O_2 0.0, H_2O 0.0, N_2 0.0, CO_2 0.75
- *Cathode*: H_2 0.0, O_2 0.23, H_2O 0.0, N_2 0.77, CO_2 0.0

At the outlets, the computed pressure is relative to the external pressure, which is considered known.

On all the walls the no-slip boundary condition is applied for the momentum equations, and the shear stress is calculated by the use of "wall-functions" [13].

The surface production and consumption rates of the products in both electrodes are involved in the special conditions for the electrochemical reactions [10].

2.1.4. Characteristics of a PAFC operation

In an operating fuel cell if all irreversible losses are taken into account, the actual cell voltage is

$$V_C = E - \Delta V_{\mathrm{losses}} \quad (6)$$

where E is the open circuit voltage (OCV) obtained by the Nernst equation and $\Delta V_{\mathrm{losses}}$ are the total voltage losses. Voltage irreversible losses can be expressed as a function of current density

Table 1
The examined fuel cell geometry

PAFC geometry	
Dimension *X*, fuel gas flow direction	30 cm
Dimension *Y*, fuel cell thickness	1 cm
Dimension *Z*, oxidant gas flow direction	20 cm

I [16]. Based on all the above considerations, the following relationship is formed:

$$V_C = E - \Delta V_{act} - \Delta V_{ohmic} - \Delta V_{conc} \quad (7)$$

where ΔV_{act}, ΔV_{ohm}, and ΔV_{conc} stand for the activation, ohmic, and concentration losses, respectively. When voltage loss terms are replaced by the respective analytical expressions, the above equation can be written as

$$V_C = E - A\ln\left(\frac{I}{I_0}\right) - Ir - m\exp(n_c I) \quad (8)$$

where A is the "Tafel constant", I is the current density, I_0 is the exchange current density, r is the area specific resistance, and m, n_c are constants.

This equation is widely used by the majority of fuel cell researchers for the estimation of final fuel cell voltage given a constant current, while the mass concentration losses are calculated by an empirical equation [17].

"Hydrogen utilization", U_f, is defined as the ratio of the hydrogen mass that reacts to the incoming hydrogen mass flow:

$$U_f = \frac{m_{H_2,react}}{m_{H_2,input}} \quad (9)$$

Faraday's first law indicates that the hydrogen mass flow that reacts is proportional to current density I, while the hydrogen mass flow that enters the system is proportional to the fuel inlet volumetric rate. Therefore, the following hydrogen utilization U_f can alternatively be expressed using the following equation:

$$U_f = \beta_f \frac{I}{Q_f} \quad (10)$$

where Q_f is the inlet fuel volumetric flow and β_f is a constant that depends on the type and geometry of each particular fuel cell as well as on the composition of fuel gas.

A similar equation to Eq. (9) defines "Oxygen utilization" U_{ox}:

$$U_{ox} = \frac{m_{O_2,react}}{m_{O_2,input}} \quad (11)$$

Similarly to Eq. (10), oxygen utilization can alternatively be defined as follows:

$$U_{ox} = \beta_{ox} \frac{I}{Q_{ox}} \quad (12)$$

where Q_{ox} is the inlet oxidant volumetric flow and β_{ox} is a constant that depends on the type and geometry of each particular fuel cell as well as on the composition of oxidant gas.

Fuel cell efficiency can be expressed by the following equation:

$$n_{eff}\ (\%) = U_f \frac{V_C}{1.25} \times 100 \quad (13)$$

where V_C is the operating fuel-cell voltage and 1.25 V is the maximum cell voltage based on the lower heating value (LHV).

2.2. Formulation of database

Eqs. (10) and (12) indicate that only three of the variables Q_f, Q_{ox}, U_f, U_{ox}, and I are independent variables. In order to obtain a database for training the linear and neural network models, we selected the fuel inlet volumetric rate Q_f, the oxidant inlet volumetric rate Q_{ox} and fuel utilization U_f as the independent input-variables and performed several runs of the CFD model. In particular, we assigned values in the range (5–80%) to fuel utilization, whereas fuel inlet volumetric rate and oxidant volumetric rates took values in the ranges (40–120 l h^{-1}) and (85–800 l h^{-1}), respectively (both volumetric rates were measured in STP).

Table 2
The database used for the generation and validation of the linear regression model and the NNM

No. of data	V_C (V)	U_f (%)	Q_f (l h^{-1})	U_{ox} (%)	Q_{ox} (l h^{-1})
1	0.748878	21	40	14.1	125
2	0.65328	47	60	46	130
3	0.614492	62	80	26	400
–	–	–	–	–	–
–	–	–	–	–	–
–	0.577843	57	120	29	500
–	–	–	–	–	–
480	–	–	–	–	–

The database that is used for both linear regression and neural network modeling consists of 480 input–output pairs and has the form shown in Table 2.

3. Development of the meta-models

This section presents the procedure that was followed in order to develop correlation equations between the cell voltage V_C and the three independent input variables Q_f, Q_{ox}, and U_f. In particular, for the linear regression method, the natural logarithms of the three independent variables are used as input parameters to the model.

3.1. Linear regression

The database that is generated by the CFD simulation results was initially used to develop an equation that correlates the cell voltage V_C with the three independent input variables Q_f, Q_{ox}, and U_f. It was found that the accuracy of the produced model is higher if the natural logarithms of the variables are utilized. Therefore, although linear regression is used, the following non-linear model between the input and the output variables was finally produced:

$$V_C = -0.094894 \times \ln(Q_f) + 0.017765 \times \ln(Q_{ox}) - 0.085789 \times \ln(U_f) + 1.2773 \quad (14)$$

The above model is associated with the following statistics:

Root mean-squared error(RMSE)

$$= \sqrt{\frac{SSE}{n-k-1}} = \sqrt{\frac{\sum_{i=1}^{n}(V_{C,i} - \hat{V}_{C,i})^2}{n-k-1}} = 0.0616 \quad (15)$$

Coefficient of determination(R^2)

$$= 1 - \frac{SSE}{SSY} = 1 - \frac{\sum_{i=1}^{n}(V_{C,i} - \hat{V}_{C,i})^2}{\sum_{i=1}^{n}(V_{C,i} - \bar{V}_C)^2} = 0.9770 \quad (16)$$

$$F\text{-statistic} = \frac{(R^2/k)}{(1-R^2)/(n-k-1)} = 6742.7 \quad (17)$$

where SSE stands for the sum of squared errors between the observations and the predicted values over the set of the available data, while SSY stands for the sum of squared deviations between the observations and their mean. In the above equations $V_{C,i}$ is the CFD cell voltage value for the ith observation, $\hat{V}_{C,i}$ is the associated model prediction, and $\bar{V}_C$ is the mean of all CFD cell voltage values in the available data set. Finally, k is the number of the independent variables, and n the number of the available input–output data.

In order to explore the reliability of the modeling methodology we also used the cross-validation method. Based on this technique, a number of modified data sets are created by deleting in each case

Table 3
Minimum, maximum, mean and standard deviation values of the RMSE and R^2 statistics obtained after performing 100 runs

	Minimum	Maximum	Mean	S.D.
RMSE	0.1028	0.1469	0.1237	0.0089
R^2	0.9712	0.9829	0.9775	0.0023

one or a small group (i.e. leave some out) of objects. For each data set, an input-output model is developed, based on the utilized modeling technique. Each model is evaluated, by measuring its accuracy in predicting the responses of the remaining data (the ones that have not been utilized in the development of the model). In particular, the leave one-out (LOO) procedure was utilized in this study, which produces a number of models, by deleting each time one object from the training set. Obviously, the number of models produced by the LOO procedure is equal to the number of available examples n. Prediction error sum of squares (PRESS) is a standard index to measure the accuracy of a modeling method using the cross-validation technique. Based on the PRESS and SSY statistics, the R^2_{CV} and S_{PRESS} values can be easily calculated. The formulae used to calculate all the aforementioned statistics are presented below:

$$R^2_{CV} = 1 - \frac{\text{PRESS}}{\text{SSY}} = 1 - \frac{\sum_{i=1}^{n}(V_{C,i} - \hat{V}^{LOO}_{C,i})^2}{\sum_{i=1}^{n}(V_{C,i} - \bar{V}_C)^2} \quad (18)$$

$$S_{PRESS} = \sqrt{\frac{\text{PRESS}}{n-k-1}} \quad (19)$$

where $\hat{V}^{LOO}_{C,i}$ is the cell voltage prediction for observation i of the model that is trained using all the available data, except from observation i. The obtained results are

$R^2_{CV} = 0.9765$
$S_{PRESS} = 0.0117$

Further validation of the linear regression methodology was performed by developing models based on 75% of the available data and evaluating them on the validation set, i.e. the rest of the database that was not used for the derivation of the model. In order to show that the success of one particular model is not due to a chance correlation, 100 random partitions of the data into training and validation sets (75% and 25% of the data, respectively) were used to derive 100 different correlation equations. The RMSE and

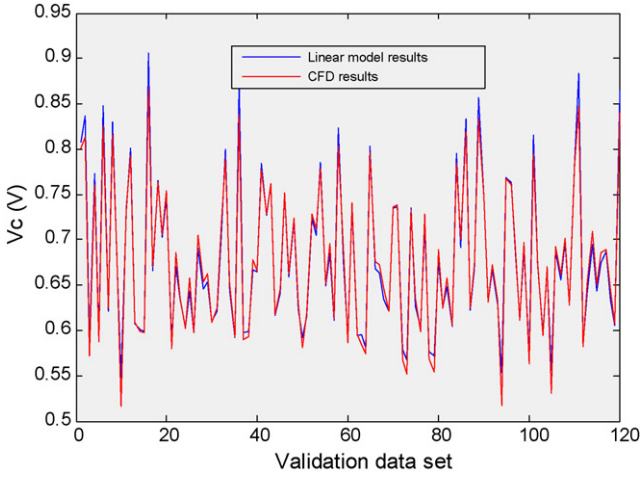

Fig. 2. CFD cell voltage values and linear model predictions for the validation dataset.

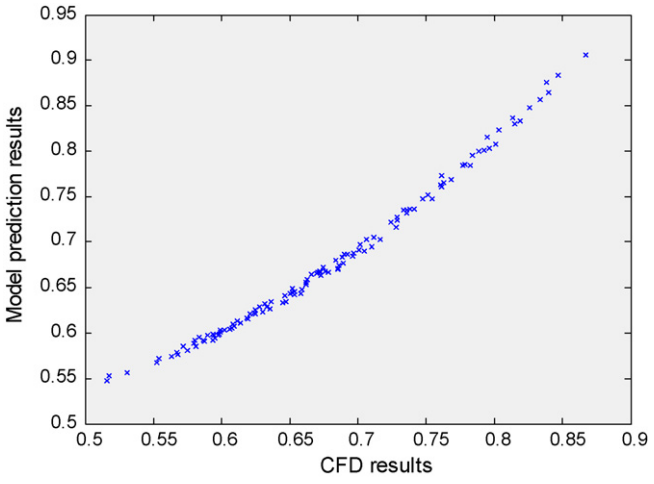

Fig. 3. CFD cell voltage values vs. linear model predictions for the validation dataset.

R^2 statistics were calculated for each model using only the validation examples. Table 3 shows the minimum, maximum, mean and standard deviation values of the RMSE and R^2 statistics obtained after performing the 100 runs.

Figs. 2 and 3 present the predicted values for V_c obtained from a linear model corresponding to RMSE = 0.1127 and R^2 = 0.9813 in comparison to the CFD simulation results. Fig. 4 compares the CFD simulation results with the linear model predictions using the LOO cross-validation procedure. It is quite obvious that the model developed using the linear regression technique is quite successful and accurate except for the cases where the values of the output variable are close to their upper or lower limits.

3.2. Neural network model (NNM)

In this section, we examine how the results presented in the previous subsection can be improved in terms of the accuracy of the produced model, by utilizing a non-linear statistical modeling approach. In particular, the radial basis function (RBF) neural network architecture is utilized for modeling the system. This specific architecture was chosen because of its simple topology and the fast and robust algorithms that are available in the literature for training such networks. The topology of the RBF network is presented in Fig. 5 and consists of three layers: the input layer, the hidden layer and the output layer.

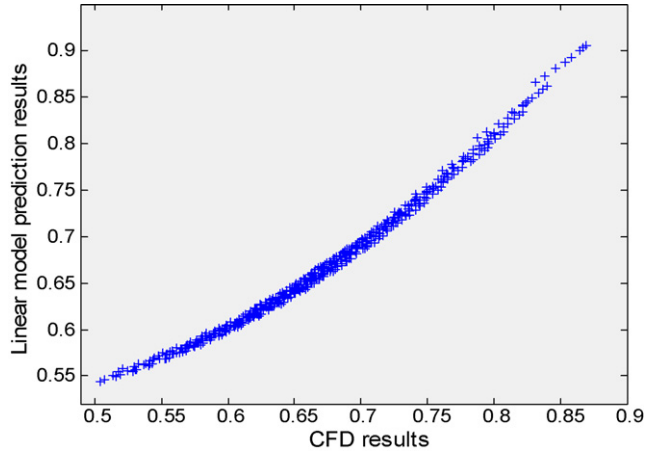

Fig. 4. CFD cell voltage values vs. linear model predictions using the cross-validation procedure.

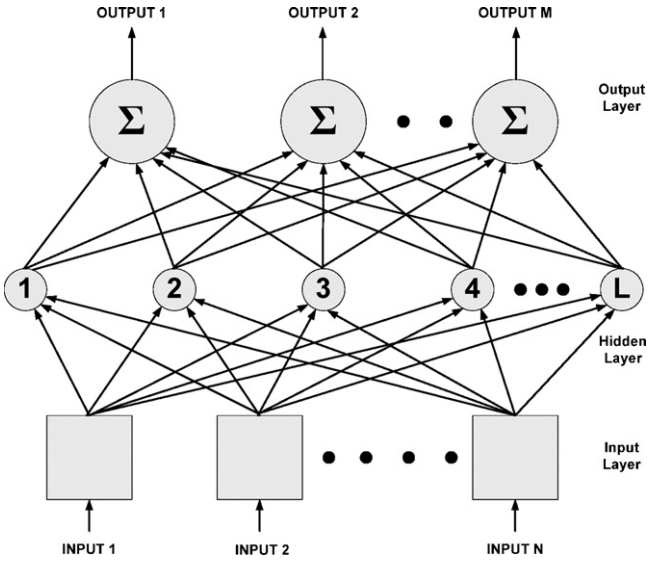

Fig. 5. Standard topology of an RBF neural network.

In this study, the RBF network is structured so that it can predict the cell voltage V_C, which is the output variable, using three independent input parameters: the fuel volumetric rate Q_f, the oxidant volumetric rate Q_{ox}, and the fuel utilization U_f. Thus, the input vector $\mathbf{x}$ is defined as $\mathbf{x} = [Q_f \ Q_{ox} \ U_f]^T$.

The neural network output provides the estimated value $\hat{V}_C$ for the cell voltage and is calculated as a weighted sum of the responses of the hidden layers:

$$\hat{V}_C = \sum_{j=1}^{L} w_j z_j(\boldsymbol{x}) \tag{20}$$

Table 4
Statistical indices corresponding to the linear model and RBF network models

	Linear model	RBF (6 fuzzy sets)	RBF (7 fuzzy sets)	RBF (8 fuzzy sets)	RBF (9 fuzzy sets)
RMSE	0.0617	0.0740	0.0342	0.0165	0.0075
R^2	0.9770	0.9861	0.9947	0.9969	0.9995
R^2_{CV}	0.9765	0.9829	0.9863	0.9946	0.9991
S_{PRESS}	0.0117	0.0101	0.0090	0.0056	0.0022

where

$$z_j(\mathbf{x}) = f\left(||\mathbf{x} - \mathbf{x}_j||_2^2\right) \tag{21}$$

In the above equations z_j is the response of the jth node, f is the radial basis function, $\mathbf{x}_j$ is the center of the jth node, L is the total number of hidden nodes and w_j is the weight corresponding to the response of the jth node.

An RBF training procedure aims at the determination of the number of nodes in the hidden layer, the hidden node centers and the output weights, in order to minimize the deviation between the predicted and the measured values of the output variables over the set of the available database. The performance of the produced network is validated on the set of input–output data that have not been utilized during the training procedure.

The training method used in this work is based on the fuzzy partition of the input space, which is produced by defining a number of triangular fuzzy sets in the domain of each input variable [18]. The centers of these fuzzy sets form a multidimensional grid on the input space. A rigorous selection algorithm chooses the most appropriate vertices on the grid, which are then used as the hidden node centers in the resulting RBF network model. The idea behind the selection algorithm is to place the centers in the multidimensional input space, so that the distance between any two center locations is guaranteed to be greater than a lower limit, which is defined by the length of the edges on the grid. At the same time, the algorithm

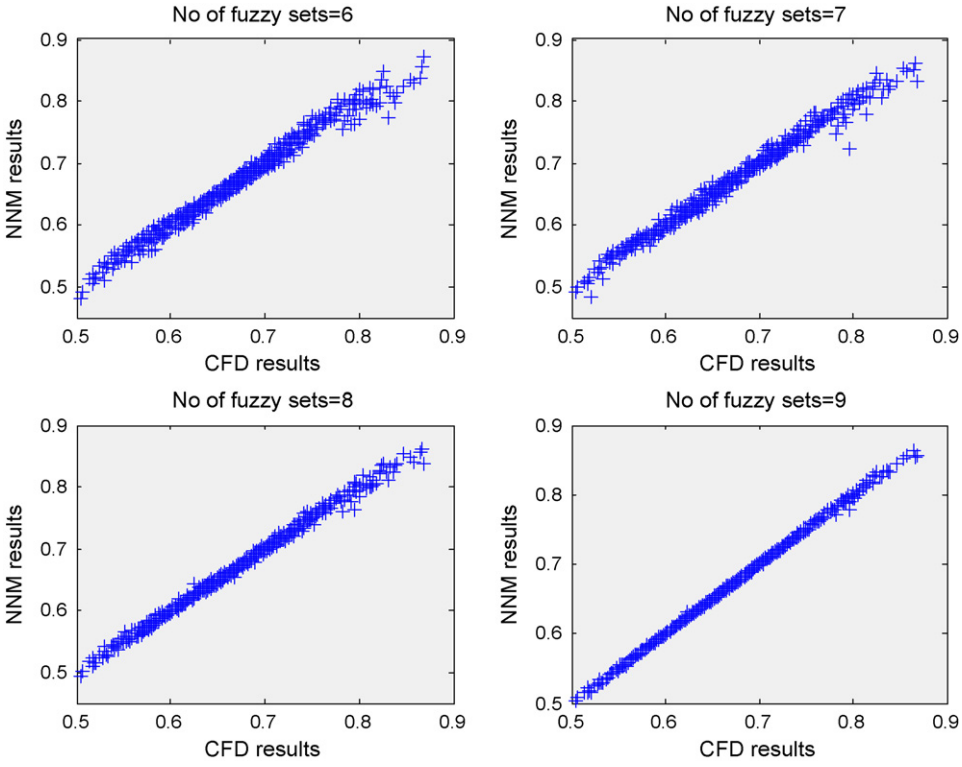

Fig. 6. CFD cell voltage values vs. neural network model predictions using the cross-validation procedure.

assures that for any input example in the training set there is at least one selected hidden node that is close enough, according to an appropriately defined distance criterion. The so-called "fuzzy-means" training method does not need the number of centers to be fixed before the execution of the method. Due to the fact that it is a one-pass algorithm, it is extremely fast, even in the case of a large database of input–output training data. One additional advantage is that the training algorithm used needs only one tuning parameter, namely the number of fuzzy sets that are utilized to partition each input dimension.

The training procedure was used several times by altering at each run the fuzzy partition of the input space (number of fuzzy sets defined in each input dimension), which is in fact the only design parameter that must be defined by the user when utilizing the fuzzy-means algorithm. Table 4 compares the statistical indices corresponding to the RBF networks with those obtained using the linear model. Fig. 6 depicts the CFD cell voltage values vs. the ones produced by the different RBF neural network models using the LOO cross-validation procedure. The average time needed to train an RBF network using an Intel Core 2.2 GHz processor was 15 s.

The RBF neural network modeling technique was further validated by developing neural network models using exactly the same 100 random partitions of the data into training and validation sets (75% and 25% of the data, respectively) that were used to test the linear approach. For each random partition, four neural network models were developed by altering the fuzzy partition of the input space. The results were gradually improved up to the point where nine fuzzy sets were used to partition the domain of each input variable. A further increase results to the overtraining phenomenon, where the performance of the produced model is not improved, although the model increases in size. The RMSE and R^2 statistics were calculated for each model using only the validation examples. Table 5 shows the minimum, maximum, mean, and standard deviation values of the RMSE and R^2 statistics obtained after performing the 100 runs and compares the results with those corresponding to the linear model.

Table 5
Minimum, maximum, mean and standard deviation values of the RMSE and R^2 statistics obtained after performing 100 runs of the RBF network methodology

	Minimum	Maximum	Mean	S.D.
Linear model				
RMSE	0.1028	0.1469	0.1237	0.0089
R^2	0.9712	0.9829	0.9775	0.0023
RBF network models				
No of fuzzy sets = 6				
RMSE	0.0801	0.3094	0.1510	0.0490
R^2	0.8602	0.99078	0.9572	0.02912
No of fuzzy sets = 7				
RMSE	0.0456	0.1183	0.0763	0.0166
R^2	0.9704	0.9969	0.9895	0.0052
No of fuzzy sets = 8				
RMSE	0.0262	0.0681	0.0400	0.0081
R^2	0.9777	0.9989	0.9667	0.0024
No of fuzzy sets = 9				
RMSE	0.0144	0.0418	0.0232	0.0049
R^2	0.9963	0.9997	0.9989	0.0005

Comparison with the results obtained from the linear modeling methodology.

Figs. 7 and 8 present the predicted values for V_c obtained from the developed RBF networks in comparison to the values obtained from the CFD simulation code. Each subfigure corresponds to different fuzzy partitions of the input space. From both visual inspection of Figs. 6–8 and the results presented in Tables 4 and 5 it becomes apparent that utilization of the RBF modeling approach indeed improved the accuracy of the produced model compared to the linear approach, mainly when cell voltage takes values which are close to the limits.

Concluding, various models have been developed in order to investigate the relationship between cell voltage and three independent input variables and the most reliable is based on neural-network techniques. Fig. 9 illustrates in 3D view the cell voltage as a function of fuel and oxidant inlet volumetric rates for

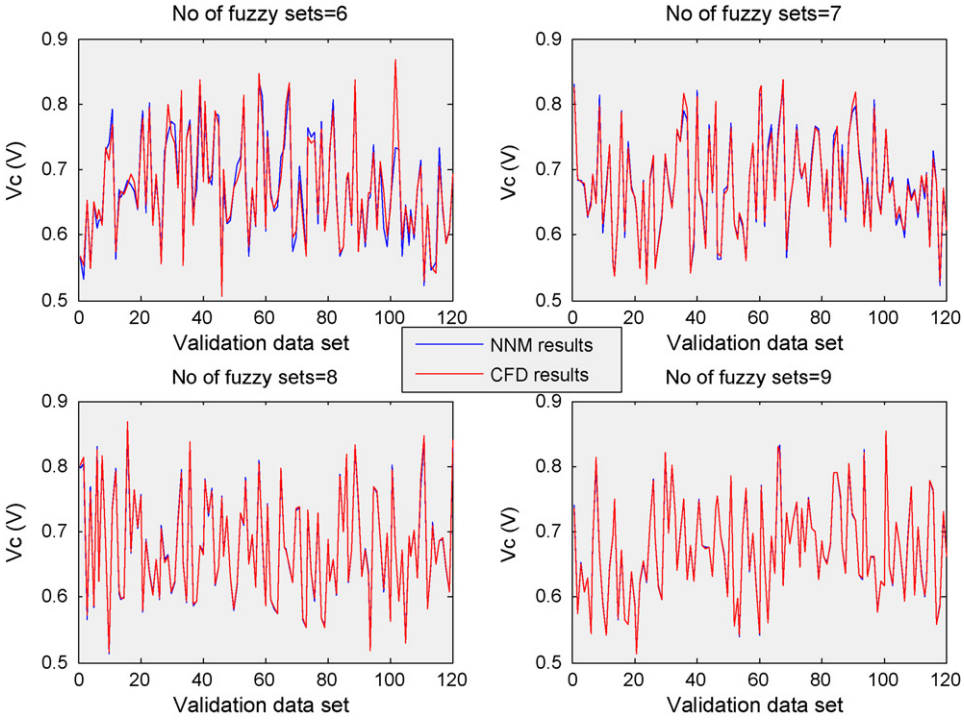

Fig. 7. CFD cell voltage values and neural network model predictions for the validation dataset.

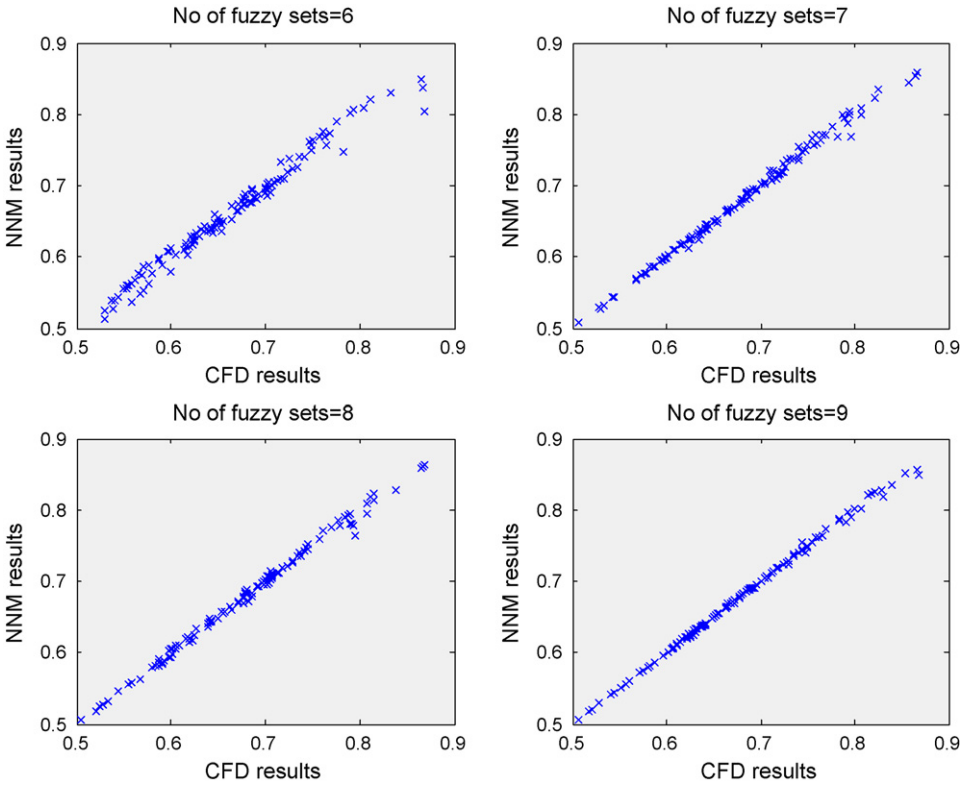

Fig. 8. CFD cell voltage values vs. neural network model predictions for the validation dataset.

discrete values of fuel gas utilization that vary between 5% and 80% in increments of 5%. The bottom surface corresponds to the highest value of U_f. The results in Fig. 9 correspond to the neural network model that was generated by considering nine fuzzy sets in each input dimension.

4. Optimization of the PAFC performance

4.1. The concept

Research in fuel cell systems has indicated that performance can be optimized by selecting appropriate fuel flow and oxidant flow set points [19]. These are not fixed, but do depend on the power that is produced by the system. In this section, we illustrate that the meta-models presented in the previous section can be utilized to compute those optimal set points. In particular, the models will be used to optimize the performance of the system that is presented in Fig. 10 for different power demands. Power is supplied by a DC/AC inverter which follows the fuel cell. The optimization problem is formulated so that it takes into account the various constraints and limitations of the system. In Section 4.2 the formulation of the optimization problem is presented in details.

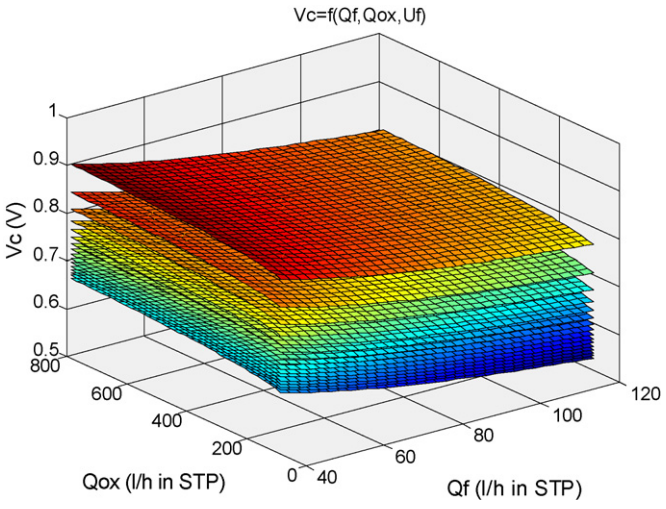

Fig. 9. Cell voltage predicted values as a function of fuel and oxidant gas inlet volumetric rates and fuel gas utilization.

4.2. Formulation of the optimization problem

This subsection describes the optimization framework which is formulated in order to obtain the optimal set points for the inlet fuel and oxidant volumetric flow rates, given a particular value of the power demand P_D. A hierarchical two-objective optimization problem is defined, where the two performance criteria are given different priorities and thus, they are optimized in a sequence and

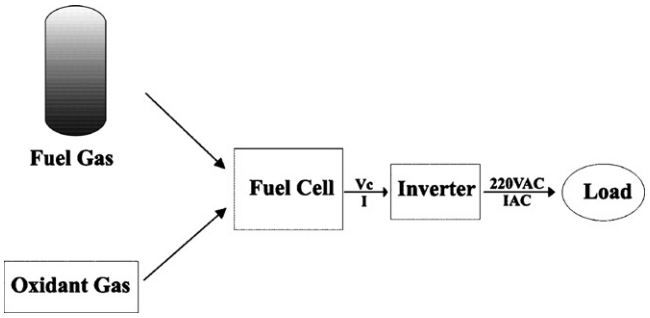

Fig. 10. Fuel cell system setup.

not in parallel. The constraints that should be satisfied by the solution of the problem are presented first, followed by the presentation of the two optimization problems.

4.2.1. Constraints

The following set of constraints are included in the formulation of both optimization problems:

(i) The cell voltage is expressed as a function of Q_f, Q_{ox}, U_f. Either of the two meta-models that were derived in Section 3 (model based on linear regression or RBF neural network model) can be utilized:

$$V_c = f(Q_f, Q_{ox}, U_f) \tag{22}$$

(ii) Fuel gas utilization is a function of current density and fuel inlet volumetric rate. We use Eq. (10), where the value that corresponds to our particular fuel cell application is assigned to the parameter β_f:

$$U_f = 2.07345 \frac{I}{Q_f} \tag{23}$$

(iii) Oxidant utilization is a function of current density and oxidant inlet volumetric rate. We use Eq. (12), where the value that corresponds to our particular fuel cell application is assigned to the parameter β_{ox}:

$$U_{ox} = 4.40123 \frac{I}{Q_{ox}} \tag{24}$$

(iv) Fuel cell output power P_C is defined as the product of fuel cell operating voltage, current density, and electrode effective area, which for the geometry of our particular application is 0.04 m^2.

$$P_C = 0.04 V_C I \tag{25}$$

(v) Finally, inverter output power – which is equal to the power demand P_D – is a function of the fuel cell output power. As discussed in Ref. [20], it is sufficient to assume a fixed inverter efficiency (90%):

$$P_D = 0.9 P_C \tag{26}$$

A number of additional constraints are used in the optimization problem to express physical limitations of the system and/or bound the system variables between desired upper and lower limits. In particular, the following upper and lower limits are posed on the cell voltage, and the fuel- and oxidant-gas inlet volumetric rates and utilizations: cell voltage (0.5–0.8 V), fuel volumetric flow rate (40–120 l h^{-1}), oxidant volumetric flow rate (85–800 l h^{-1}), fuel utilization (5–80%), and oxidant utilization (10–70%).

4.2.2. Objective functions

Selection of the objective function is a critical issue in the formulation of the optimization problem. The two key variables that should be present in the objective function to be minimized are the volumetric rates of the oxidant and fuel gases. As mentioned previously, we construct the optimization problem using a multi-objective hierarchical approach. In the first step we minimize the fuel volumetric rate Q_f, recognizing the fact that our first concern is to minimize consumption of the expensive fuel. In the second step we optimize with respect to the oxidant volumetric rate Q_{ox}. This is considered as a second-priority but still important objective, because by lowering Q_{ox} we actually reduce the parasitic compressor power, which in turn increases the net power of the fuel cell system. The result of the first step is added as a constraint in the second step, but we allow a slight increase in the optimal value of Q_f as it is explained next.

- First stage:
  The first optimization problem is formulated as follows:

$$\min_{Q_f, Q_{ox}, U_f, U_{ox}, I, V_C} Q_f \tag{27}$$

  subject to the constraints (22)–(26) and the upper and lower bounds posed on the variables of the problem.
- Second stage:
  If we denote the optimal result of the first stage by Q_f^1, the second optimization problem is defined as follows:

$$\min_{Q_f, Q_{ox}, U_f, U_{ox}, I, V_C} Q_{ox} \tag{28}$$

  subject to the constraints (22)–(26), the upper and lower bounds posed on the variables of the problem and the following additional constraint:

$$Q_f \le Q_f^1 (1 + \theta\%) \tag{29}$$

  which ensures that the optimal result of the first stage regarding the fuel volumetric rate is not deteriorated by more than θ%. A typical value for the parameter θ% which is also used in the results that are presented next is 5%.

4.2.3. Type of optimization problem

The neural network model derived in Section 3.2 is obviously non-linear. However, even in the case when the model derived by linear regression is used to correlate V_c with the independent input variables Q_f, Q_{ox}, U_f, the relationship is non-linear (the natural logarithms of the input variables are used). Thus, the mathematical programming problems that are formulated in both stages of the proposed methodology are non-linear.

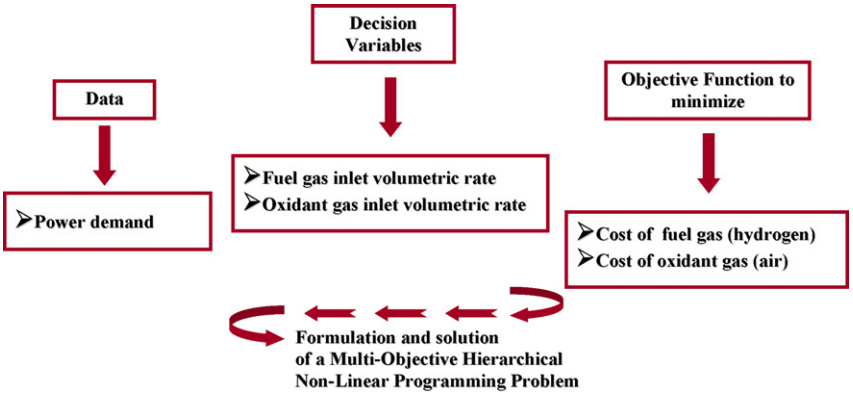

Fig. 11. Formulation of the multi-objective Non-Linear Programming Problem.

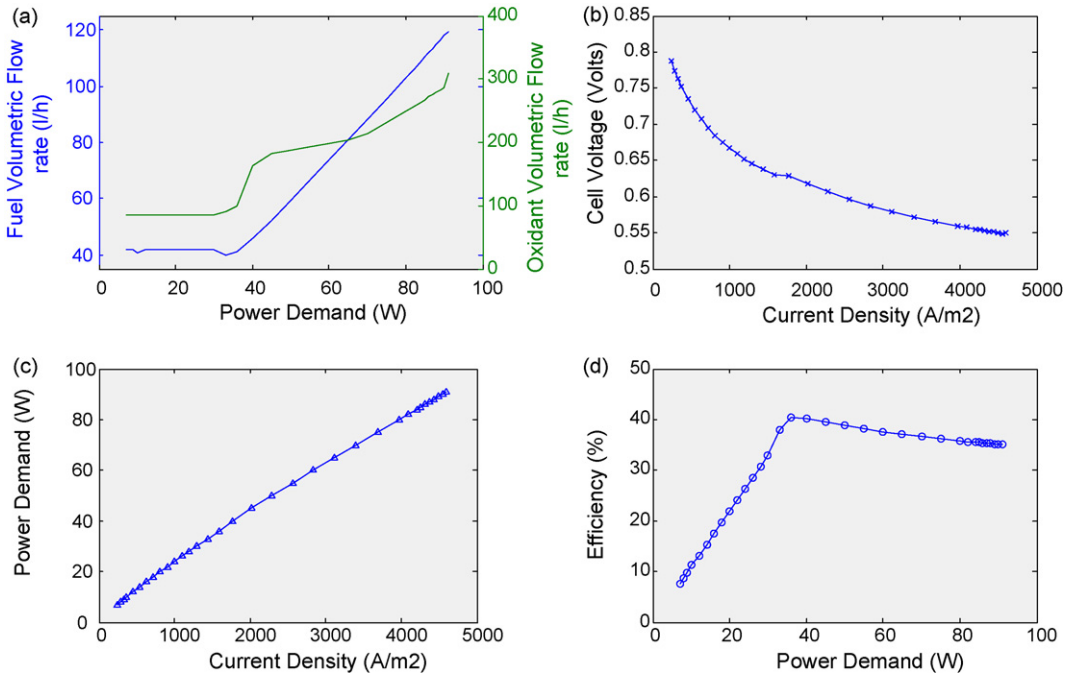

Fig. 12. (a) Optimal values of fuel and oxidant inlet volumetric rates as a function of power demand, (b) optimal values of cell voltage as a function of current density, (c) optimal values of power demand as a function of current density and (d) optimal values of FC efficiency as a function of power demand.

The non-linear programming (NLP) problems are solved using GAMS [21], which is a powerful commercial modeling language. The solution of the second stage provides the final optimal values of the fuel and oxidant volumetric rates Q_f^*, Q_{ox}^* (which are the manipulated variables in a real application), but also the optimal values of the cell voltage V_C^*, the current density I^* and the hydrogen and oxygen utilizations U_f^*, U_{ox}^*. The optimal values of power density, PD*, and the PAFC efficiency, n_{eff}^*, can be easily obtained next (for example Eq. (13) can be used for the calculation of optimal efficiency). The complete optimization problem that is formulated is summarized in Fig. 11.

4.3. Solution of the optimization problem—results

In this subsection, we present the results obtained from the solution of the proposed multi-objective NLP optimization framework that is proposed in this work. The results have been obtained using the neural network model that was developed, by considering 9 fuzzy sets in each input dimension which was the most reliable and accurate among all the meta-models that have been presented in Section 3. We ran the optimization tool for different values of power demand covering the range (5–90 W) and for each value we obtained the optimal values of fuel and oxidant inlet volumetric rates, cell voltage, current density, cell power density, and efficiency. The results are presented graphically in Fig. 12. The average time required to solve the multi-objective optimization problem in an Intel Core 2.2 GHz processor was 2.8 min when utilizing the neural network model. This is much higher compared to the average time needed to solve the problem when incorporating the model based on linear regression, which was 9 s.

In Fig. 12, we can notice a jump in the optimal oxidant volumetric flow rate Q_{ox}^* and a change in the slope of the optimal efficiency curve when power demand P_D becomes equal to 38 W. This happens because at this particular value of P_D, the optimal value of fuel utilization U_f^* hits for the first time its upper limit (80%). The power demand can then be met only by increasing substantially the oxidant fuel rate Q_{ox}^* (this is obtained as the result of the second optimization stage). The change in the slope of the efficiency curve is explained by observing that up to the specific value of power demand of 38 W, optimal fuel utilization U_f^*, which affects efficiency according to Eq. (13), is constantly increasing. For greater values of power demand, U_f^* remains fixed at its upper limit and thus efficiency changes only due to changes in cell voltage values.

5. Conclusions

In this work a PAFC optimization study has been performed, based on meta-models that were derived by applying two regression methods on the results produced by a CFD model:

- Linear regression methodology.
- The RBF neural network methodology.

The linear regression methodology leads to a model where the natural logarithms of the input variables are linearly combined to predict the cell voltage. The produced model is not accurate enough for output values which are close to the upper or lower limits. However, the reliability of the linear regression methodology is quite satisfactory for the rest of the output range. Several statistical tests illustrated the superiority of the neural network model in terms of accuracy, especially in the cases where the output variables take values close to their upper or lower limits.

The optimization study is based on the formulation of a multi-objective Non-Linear Programming Problem, that takes into account several constraints and physical limitations of the system. The solution of the optimization problem provides the optimal values of the process variables, given the power demand. A main result of this study is the nomograms that depict the optimal values of the manipulated variables (fuel and oxidant inlet volumetric rates) as functions of power demand. These optimal values can be used as targets in real time flow control loops.

The proposed computational tool is system specific, i.e. different nomograms will be constructed by applying the method for different types of fuel cells and/or different cell geometries.

Therefore, the results are subject to further development and exploitation. The proposed computational tool could additionally be further validated by applying it in a real PAFC system comprised of the components shown in Fig. 10.

An extension of the approach described in this paper, which is under development, will add dynamic characteristics to the produced models. The dynamic models will serve as dynamic simulators, but they will also be utilized as predictors of the future temporal behavior of the process in a model predictive control framework.

In conclusion, the proposed methodology may prove to be a very useful tool for researchers and practitioners who are interested in fuel cell systems and their applications, as it integrates and combines different modeling and optimization approaches, starting from a detailed and analytical model of the system and reaching finally to the process of optimal decision making regarding the operation of the system.

Acknowledgment

P.L. Zervas acknowledges the research committee of the National Technical University of Athens for financial support.

References

[1] G.H. Guvelioglu, H.G. Stenger, J. Power Sources 147 (2005) 95–106.
[2] R. Sousa Jr., E.R. Gonzalez, J. Power Sources 147 (2005) 32–45.
[3] C.H. Cheng, K. Fei, C.W. Hong, Computers Chem. Eng. 31 (2007) 247–257.
[4] P.L. Zervas, A. Tatsis, H. Sarimveis, M.K. Koukou, N.C. Markatos, in: P.V. Alemo (Ed.), Progress in Fuel Cell Research, Nova Science Publishers, New York, 2007, pp. 147–214.
[5] J. Wu, Q. Liu, H. Fang, J. Power Sources 156 (2006) 388–399.
[6] S. Ou, L.E.K. Achenie, J. Power Sources 140 (2005) 319–330.
[7] S.O.T. Ogaji, R. Singh, P. Pilidis, M. Diacakis, J. Power Sources 154 (2006) 192–197.
[8] C. Nitsche, S. Schroedl, W. Weiss, E. Pucher, J. Power Sources 145 (2005) 383–391.
[9] W.Y. Lee, G.G. Park, H.T. Yang, Y.G. Yoon, C.S. Kim, Int. J. Hydrogen Energy 29 (2004) 961–966.
[10] P.L. Zervas, M.K. Koukou, N.G. Orfanoudakis, N.C. Markatos, Proc. Inst. Mech. Eng. A: J. Power Energy 220 (2006) 525–533.
[11] M. Ghouse, H. Abaoud, A. Al-Boeiz, M. AbdulHadi, Appl. Energy 60 (1998) 153–167.
[12] S.V. Patankar, Numerical Heat Transfer and Fluid Flow, McGraw-Hill, New York, 1980.
[13] N.C. Markatos, Ironmaking Steelmaking 16 (1989) 266–273.
[14] R.H. Perry, D.W. Green, Perry's Chemical Engineering Handbook, seventh ed., McGraw Hill, New York, 1999.
[15] R.C. Reid, J.M. Prausnitz, B.E. Poling, The Properties of Gases and Liquids, McGraw Hill, New York, 1988.
[16] J. Larminie, A. Dicks, Fuel Cell Systems Explained, second ed., John Wiley & Sons Ltd., New York, 2003.
[17] J. Kim, S.M. Lee, S. Srinivasan, J. Electrochem. Soc. 142 (1995) 2670–2674.
[18] H. Sarimveis, A. Alexandridis, G. Tsekouras, G. Bafas, Ind. Eng. Chem. Res. 41 (2002) 751–759.
[19] J.T. Pukrushpan, A.G. Stefanopoulou, H. Peng, Control of Fuel Cell Power Systems, Springer, 2004.
[20] P.L. Zervas, H. Sarimveis, J.A. Palyvos, N.C. Markatos, J. Power Sources 181 (2008) 327–338.
[21] A. Brooke, D. Kendrick, A. Meeraus, R. Raman, GAMS, User Guide, 1998, Available with the GAMS system or from http://www.gams.com.